

The effect of non-linear mutual friction on pulsar glitch sizes and rise times

T. Celora^{1*}, V. Khomenko², M. Antonelli^{2†}, B. Haskell^{2‡}

¹*Mathematical Sciences and STAG Research Centre, University of Southampton, Southampton SO17 1BJ, UK*

²*Nicolaus Copernicus Astronomical Center of the Polish Academy of Sciences, ul. Bartycka 18, 00-716 Warsaw, Poland*

21 December 2024

ABSTRACT

Observations of pulsar glitches have the potential to provide constraints on the dynamics of the high density interior of neutron stars. However, to do so, realistic glitch models must be constructed and compared to the data. We take a step towards this goal by testing non-linear models for the mutual friction force, which is responsible for the exchange of angular momentum between the neutron superfluid and the observable normal component in a glitch. In particular, we consider a non-linear dependence of the drag force on the relative velocity between superfluid vortices and the normal component, in which the contributions of both kelvin and phonon excitations are included. This non-linear model produces qualitatively new features, and is able to reproduce the observed bimodal distribution of glitch sizes in the pulsar population. The model also suggests that the differences in size distributions in individual pulsars may be due to the glitches being triggered in regions with different pinning strengths, as stronger pinning leads to higher vortex velocities and a qualitatively different mutual friction coupling with respect to the weak pinning case. Glitches in pulsars that appear to glitch quasi-periodically with similar sizes may thus be due to the same mechanisms as smaller events in pulsars that have no preferred glitch size, but simply originate in stronger pinning regions, possibly in the core of the star.

Key words: stars: neutron - stars: rotation - pulsars: general

1 INTRODUCTION

Neutron stars (NSs) are promising environments in which to study physics in extreme conditions, and a significant amount of work has been devoted to using electromagnetic (see e.g. [Bogdanov et al. 2019](#)) and gravitational observations ([Abbott et al. 2018](#)) to constrain the equation of state (EOS) of dense matter in the interior of these objects. These studies are complementary to those that can be carried out with terrestrial experiments, as particle accelerators and heavy ion colliders cannot probe the high density and low temperature behaviour of the fundamental interactions, nor study the behaviour of matter with the large isospin asymmetries that characterize NS interiors ([Haensel et al. 2007](#)). In particular the neutrons are expected to be superfluid at such densities and temperatures ([Haskell & Sedrakian 2017](#); [Chamel 2017](#)).

Pulsar glitches (sudden spin-ups observed in otherwise

spinning down pulsars) are thought to represent a probe into the behaviour of the superfluid interior. Most models, in fact, assume that vortices in the superfluid are pinned ([Anderson & Itoh 1975](#)), either in the crust or core of the star, and that their sudden unpinning leads to rapid transfer of angular momentum and observed glitch (see e.g. [Haskell & Melatos 2015](#)). In these models the dissipative interaction between the superfluid and normal (observable) fluid is given by the so-called ‘mutual friction’ ([Hall & Vinen 1956](#); [Bekarevich & Khalatnikov 1961](#); [Langlois et al. 1998](#); [Andersson et al. 2006](#)), which is mediated by the interaction between vortices and the normal component of the star and sets the observed coupling timescale ([Alpar & Sauls 1988](#)).

Recent observations of glitches in the Crab ([Lyne et al. 2015](#); [Shaw et al. 2018](#)) and the Vela ([Palfreyman et al. 2018](#)) pulsars have been used to obtain constraints on the mutual friction coefficients ([Haskell et al. 2018a](#); [Ashton et al. 2019](#)), which can shed light on the microscopic interaction occurring in the star and, ultimately, on the physical region the glitch is triggered. This is an interesting point, as calculations of entrainment parameters in the crust show that these may be very large ([Carter et al. 2006](#); [Chamel 2012](#)),

* T.Celora@soton.ac.uk

† mantonelli@camk.edu.pl

‡ bhaskell@camk.edu.pl

i.e. there may be very few conduction neutrons in the crust, reducing the amount of angular momentum that can be exchanged and challenging a crustal interpretation of glitches (Andersson et al. 2012; Chamel 2013; Delsate et al. 2016). In this case, part of the core superfluid, in which neutron vortices can pin to proton flux tubes (Muslimov & Tsygan 1985; Srinivasan et al. 1990; Ruderman et al. 1998; Alpar 2017) may be involved, and glitch observations could be used to constrain superfluid gap models, pinning forces and the EOS (Ho et al. 2015; Pizzochero et al. 2017; Montoli et al. 2020).

Furthermore, the distribution of glitch sizes appears to be bimodal (Fuentes et al. 2017), and some pulsars, such as Vela and the X-ray pulsar J0537-6910 appear to have mostly large glitches that occur quasi periodically (Antonopoulou et al. 2018), as opposed to most other pulsars for which the size distribution is consistent with a power law and the waiting time distribution with an exponential (Melatos & Peralta 2007; Howitt et al. 2018). This difference is also likely to be the hallmark of different physical regimes of the process (Fulgenzi et al. 2017) and possibly due to glitches originating in different physical regions of the star (Haskell & Antonopoulou 2014).

A careful determination of mutual friction parameters in the core and crust of the star, and a study of the system’s hydrodynamical response is crucial in order to make theoretical predictions. In the core of the star mutual friction is thought to be mainly due to electron scattering off magnetised vortex cores (Alpar et al. 1984), while in the crust energy is dissipated mainly by phonon excitations of the lattice (Jones 1990a) and kelvin excitations of the vortices themselves (Epstein & Baym 1992; Jones 1992), which can also occur when vortices cross flux tubes in the core (Ruderman et al. 1998; Link 2003; Glampedakis et al. 2011). Significant uncertainties still remain in the determination of crustal mutual friction parameters, which in turn impact on predictions of the glitch rise time and observed size (Haskell et al. 2012; Antonelli & Pizzochero 2017; Sourie et al. 2017). A recent step forward was taken by Graber et al. (2018) who, following the approaches of Epstein & Baym (1992) and Jones (1992), calculated the kelvin friction parameters at different densities in the crust and compared the results to Vela glitches.

In this paper we include an additional ingredient in the calculation which, we show, has a strong impact, both qualitative and quantitative, on the glitch features, namely the dependence of the mutual friction parameters on the relative velocity between superfluid vortices and the normal component. This issue is of fundamental importance in the crust, as kelvin mutual friction depends strongly on the relative velocity (Epstein & Baym 1992; Jones 1992) and is suppressed for low velocities, at which phonon contributions dominate (Jones 1990a; Jones 1990b). If vortices unpin and initially move at large velocities, they will thus experience a varying drag as the system relaxes towards equilibrium. The problem is, however, of more general relevance, as relative motions between the superfluid and normal components may lead to turbulence (Andersson et al. 2007; Peralta et al. 2006) and also to a different velocity dependence of the mutual friction parameters, as is, for example, well known for objects falling through the atmosphere on Earth, for which the terminal velocity can be obtained by considering a drag that

scales with the square of the velocity, rather than linearly as would be expected if the air flow were laminar.

In the following we first examine in the problem of mutual friction in the case of velocity dependent parameters, and discuss the different possible physical regimes. We then move on to discuss the mutual friction in the crust of a neutron star, and present a model which includes both kelvin and phonon contributions. We show that this model predicts a qualitatively different rise than standard mutual friction models, which is consistent with recent observations of a glitch in the Vela pulsar (Palfreyman et al. 2018; Ashton et al. 2019). We also apply the model to a population of glitching pulsars and show that it produces a bimodal glitch size population that has an excess of large glitches.

2 MUTUAL FRICTION: LINEAR DRAG IN ABSENCE OF TURBULENCE

Let us begin our analysis by reviewing the standard derivation of the mutual friction force in neutron stars (Mendell 1991; Carter & Chamel 2005; Andersson et al. 2006). Following Prix et al. (2002), we deal with a system composed of a charge neutral mixture of protons and electrons and everything coupled to it on short timescales (so that we can treat them as a single component, the ‘normal’ one hereafter dubbed “p”) plus a superfluid neutron component (hereafter dubbed “n”) which, due to the stellar rotation, is threaded by an array of quantized vortices.

In the absence of interactions between the superfluid and the normal component, the vortex line velocity \mathbf{v}_L is equal to the bulk velocity \mathbf{v}_n of the neutrons (where both \mathbf{v}_L and \mathbf{v}_n are orthogonal to the vortex line, see e.g. Donnelly 1991). This result can be understood by analysing the forces acting on a vortex, which to a very good degree of approximation can be treated as a massless object (Baym & Chandler 1983; Sonin 1987; Donnelly 1991), although see Simula (2018) for a recent discussion on the effective mass of a quantum vortex. In this case the only force acting on a free vortex line is the Magnus force \mathbf{f}_M per unit length of vortex,

$$\mathbf{f}_M^i = \rho_n \varepsilon^{ijk} \kappa_j (v_k^L - v_k^n), \quad (1)$$

where ρ_n is the density of neutrons and $\boldsymbol{\kappa}$ is a vector aligned locally with the vorticity, such that $\boldsymbol{\kappa} = \kappa \hat{\boldsymbol{\kappa}}$ and $\kappa = h/2m_n$ is the quantum of circulation. The requirement of force balance leads to $\mathbf{f}_M = 0$ and thus $\mathbf{v}_L = \mathbf{v}_n$. In the more general case in which the vortices interact also with the normal component flowing with velocity \mathbf{v}_p , the vortex velocity \mathbf{v}_L will in general differ from both \mathbf{v}_n and \mathbf{v}_p .

If we describe the dissipative interaction between the vortices and the normal component in terms of a linear drag force, the equation of motion of a single vortex line is

$$\mathbf{f}_M^i + \mathbf{f}_D^i = 0, \quad (2)$$

with the drag force per unit length defined as:

$$\mathbf{f}_D^i = -\eta (v_L^i - v_p^i). \quad (3)$$

The drag coefficient η is related to the dimensionless quantity \mathcal{R} often used in the literature via $\mathcal{R} = \eta/\kappa\rho_n$. It is useful to work in the normal component rest frame where

the eq. (2) reads

$$\hat{\kappa} \times (\mathbf{v}_{\text{LP}} - \mathbf{v}_{\text{np}}) - \mathcal{R} \mathbf{v}_{\text{LP}} = 0. \quad (4)$$

We can solve this equation to write the vortex velocity $\mathbf{v}_{\text{LP}} = \mathbf{v}_{\text{L}} - \mathbf{v}_{\text{p}}$ in terms of the lag $\mathbf{v}_{\text{np}} = \mathbf{v}_{\text{n}} - \mathbf{v}_{\text{p}}$, namely

$$\mathbf{v}_{\text{LP}} = -\frac{\mathcal{R}}{1 + \mathcal{R}^2} \hat{\kappa} \times \mathbf{v}_{\text{np}} - \frac{1}{1 + \mathcal{R}^2} \hat{\kappa} \times (\hat{\kappa} \times \mathbf{v}_{\text{np}}). \quad (5)$$

In the limit of “weak drag”, $\mathcal{R} \ll 1$, one can neglect the first term to get $\mathbf{v}_{\text{LP}} \approx -\hat{\kappa} \times (\hat{\kappa} \times \mathbf{v}_{\text{np}})$, as expected for the no-drag case. On the other hand, if we consider the “super strong drag” regime, that is $\mathcal{R} \gg 1$, the previous equation gives $\mathbf{v}_{\text{LP}} \approx 0$, implying that the vortex is effectively pinned.

Now, the force per unit volume acting between the normal component and the superfluid is found by averaging over all the vortices in the fluid element, or rather over the total length of vortex lines L in the element. In general this depends on the nature of the flow, as a turbulent flow can tangle the vortices and increase the length of vortex in an element (Vinen 1957; Schwarz 1988). We will discuss this possibility in the following sections. In the case of an array of straight and aligned vortices, it is possible to introduce the vortex density n_v on a unit surface orthogonal to orthogonal to $\hat{\kappa}$ and use it to get the averaged force per volume element. Then, using Newton’s third law, the force per unit volume between the vortices and the fluids can be included in the hydrodynamical equations (the full form will be given in (34)) as

$$\begin{aligned} \rho_n \partial_t \mathbf{v}_n + \dots &= -n_v \mathbf{f}_M \\ \rho_p \partial_t \mathbf{v}_p + \dots &= -n_v \mathbf{f}_D. \end{aligned} \quad (6)$$

From eq. (6) we can read the mutual friction force \mathbf{F}_{MF} , defined as the force exerted by the normal component on the superfluid, namely

$$\mathbf{F}_{MF}^i = -n_v f_M^i = n_v f_D^i, \quad (7)$$

where the vortex density n_v can be seen as a measure of the macroscopic vorticity ω_n^i vector via

$$\omega_n^i = m_n^{-1} \varepsilon^{ijk} \partial_j p_k^n = \kappa n_v \hat{\kappa}^i. \quad (8)$$

Therefore, the mutual friction force can be written in such a way that only macroscopic hydrodynamical quantities appear (Andersson et al. 2006)

$$\mathbf{F}_{MF} = \rho_n \left(\mathcal{B}_c \boldsymbol{\omega}_n \times \mathbf{v}_{\text{np}} + \mathcal{B}_d \hat{\boldsymbol{\omega}}_n \times (\boldsymbol{\omega}_n \times \mathbf{v}_{\text{np}}) \right), \quad (9)$$

where $\hat{\boldsymbol{\omega}}_n = \hat{\kappa}$ and

$$\mathcal{B}_c = \frac{\mathcal{R}^2}{1 + \mathcal{R}^2} \quad \mathcal{B}_d = \frac{\mathcal{R}}{1 + \mathcal{R}^2}. \quad (10)$$

Therefore, the mutual friction force is composed of a Coriolis-like part which is proportional to \mathcal{B}_c , and a dissipative part proportional to \mathcal{B}_d .

3 VORTEX MOTION WITH NON-LINEAR DRAG

In this section we consider the more general case of a non-linear drag force. In the standard picture, presented in the previous section, the drag parameter \mathcal{R} is taken to be a constant, which can be estimated via microphysical calculations of energy dissipation rates in specific channels. For

instance, in the NS crust, for some relatively high values of the vortex velocity $v_{\text{LP}} \gtrsim 10^4 \text{ cm s}^{-1}$, energy is dissipated mainly by Kelvin waves propagating along the vortex line (Epstein & Baym 1992). On the other hand, for lower vortex velocities the Kelvin waves are suppressed and energy is dissipated via excitation of phonons in the crustal lattice (Jones 1990a). Hence, the drag parameter \mathcal{R} itself depends on $|v_{\text{LP}}|$ (see Jones 1992). As a result, we are interested in dealing with the more general case in which the additional dependence of the drag force on the relative speed $|\mathbf{v}_{\text{LP}}|$ is encoded in $\tilde{\mathcal{R}}$,

$$f_D^i = -\rho_n \kappa \tilde{\mathcal{R}} v_{\text{LP}}^i, \quad \tilde{\mathcal{R}} = \tilde{\mathcal{R}}(|\mathbf{v}_{\text{LP}}|). \quad (11)$$

Of course, the linear drag case is recovered once $\tilde{\mathcal{R}}$ is assumed to be a constant.

While the case we are explicitly considering is that of a straight vortex array and a velocity dependent drag parameter $\tilde{\mathcal{R}}$, so that the mutual friction force can be written

$$F_{MF}^i = -n_v \rho_n \kappa \tilde{\mathcal{R}} v_{\text{LP}}^i \quad (12)$$

this is mathematically equivalent to considering a turbulent tangle of vortices, with vortex length per unit volume $\tilde{L} = \tilde{L}(|\mathbf{v}_{\text{LP}}|)$. In this latter case, the mutual friction force takes the form

$$F_T^i = -\tilde{L} \rho_n \kappa \mathcal{R} v_{\text{LP}}^i, \quad (13)$$

which is formally the same as eq. (12). The conclusions we will obtain in the following for different functional dependence of $\tilde{\mathcal{R}}$ on the vortex line velocity can thus be directly applied to the case in which \tilde{L} has the same dependence, so that e.g. the qualitative behaviour of the coupling for $\tilde{\mathcal{R}} \propto |\mathbf{v}_{\text{LP}}|^2$ can be applied to the standard case of fully developed isotropic quantum turbulence in which $\tilde{L} \propto |\mathbf{v}_{\text{LP}}|^2$ (Vinen 1957; Andersson et al. 2007).

To proceed it is useful to introduce the usual cylindrical coordinates system $(\hat{e}_x, \hat{e}_\varphi, \hat{e}_z)$ where the z-axis is aligned with the vortices, i.e. $\hat{\kappa} = \hat{e}_z$. We also consider the velocities of the two components to be azimuthal, so that $\mathbf{v}_{\text{np}} = x \Omega_{\text{np}} \hat{e}_\varphi$. On the timescales of the observable glitch dynamics this is true for a fluid element (at least on average), and allows us to simplify the analysis. However, on shorter timescales vortex accumulation (Khomenko & Haskell 2018) and counterflow along the axis of a vortex due to bending (Khomenko et al. 2019) may give rise to instabilities leading to turbulence or vortex avalanches.

In components, the force balance eq. (2) gives

$$\begin{aligned} v_{\text{LP}}^\varphi - v_{\text{np}}^\varphi + \tilde{\mathcal{R}} v_{\text{LP}}^x &= 0 \\ v_{\text{LP}}^x - \tilde{\mathcal{R}} v_{\text{LP}}^\varphi &= 0, \end{aligned} \quad (14)$$

that can be rearranged as

$$v_{\text{LP}}^x = \frac{\tilde{\mathcal{R}}}{1 + \tilde{\mathcal{R}}^2} v_{\text{np}}^\varphi = \mathcal{B}_{MF} v_{\text{np}}^\varphi. \quad (15)$$

This expression is only formal since we have that the drag parameter $\tilde{\mathcal{R}}$ still has an implicit dependence on $|\mathbf{v}_{\text{LP}}|$. The solution in eq. (15) also defines the mutual friction coefficient \mathcal{B}_{MF} , which is introduced in such a way that it reduces to \mathcal{B}_d in the linear drag case (when $\tilde{\mathcal{R}}$ is a constant).

The last equation we need is the radial component of

the vortex line velocity,

$$v_{Lp}^\varphi = \frac{v_{np}^\varphi}{1 + \tilde{\mathcal{R}}^2}. \quad (16)$$

Combining eq. (15) and eq. (16) we obtain

$$|\mathbf{v}_{Lp}| = \frac{|\mathbf{v}_{np}|}{\sqrt{1 + \tilde{\mathcal{R}}^2}} \quad (17)$$

which, given a functional dependence of $\tilde{\mathcal{R}}^2$ on $|\mathbf{v}_{Lp}|$, can be solved to eliminate the vortex line velocity from the hydrodynamical equations in eq. (6). We will analyse specific forms of the mutual friction in the following, but let us note here that eq. (17) shows that the difference between $|\mathbf{v}_{Lp}|$ and $|\mathbf{v}_{np}|$ is of $\mathcal{O}(\tilde{\mathcal{R}}^2)$, so that to very good approximation one can take $|\mathbf{v}_{Lp}| \approx |\mathbf{v}_{np}|$ for $\tilde{\mathcal{R}} \ll 1$, and simply solve the hydrodynamical equations in eq. (6) directly for $\tilde{\mathcal{R}}(|\mathbf{v}_{Lp}|) \approx \tilde{\mathcal{R}}(|\mathbf{v}_{np}|)$ (or equivalently, if dealing with turbulence, for $\tilde{L}(|\mathbf{v}_{Lp}|) \approx \tilde{L}(|\mathbf{v}_{np}|)$).

3.1 Power Law drag

Let us start with a simple prescription, and consider a power law behaviour for the drag force,

$$f_D^i = -\eta_\beta |\mathbf{v}_{Lp}|^\beta v_{Lp}^i, \quad (18)$$

where the physical dimension of the viscous parameter η_β depends on the explicit value of β . Despite its simplicity, this prescription is applicable to several physical setups. For example, in the presence of classical turbulence one has $\beta = 1$ (the standard case of objects moving in a fluid at high Reynolds number, according to Newton's drag law), and for isotropic quantum turbulence $\beta = 2$, although polarized turbulence is likely to require the use of multiple power laws to describe the drag (Andersson et al. 2007; Mongiovì & Jou 2007). Negative values of β do not have an hydrodynamical interpretation, but microphysical calculations of Kelvin drag in the crust (Jones 1992; Epstein & Baym 1992; Graber et al. 2018) and also core of the star if the protons are in a type-II superconducting state (Link 2003; Haskell et al. 2014), suggest that $\beta = -3/2$: this case is of particular interest for NSs and will be considered in detail in the following.

To work with a dimensionless drag parameter \mathcal{R} we introduce a microscopic parameter v_0 (with the dimension of a velocity) and rewrite the drag force in eq. (18) as

$$f_D^i = -\kappa \rho_n \mathcal{R} \left(\frac{|\mathbf{v}_{Lp}|}{v_0} \right)^\beta v_{Lp}^i, \quad (19)$$

where the constant and dimensionless drag parameter is $\mathcal{R} = \eta_\beta v_0^\beta / \kappa \rho_n$. In terms of the drag coefficient $\tilde{\mathcal{R}}$ previously introduced we have that

$$\tilde{\mathcal{R}} = \left(\frac{|\mathbf{v}_{Lp}|}{v_0} \right)^\beta \mathcal{R}. \quad (20)$$

Now, to solve the equations of motion for the vortex line it is helpful to introduce the dimensionless variables

$$s = \frac{v_{Lp}^\varphi}{|\mathbf{v}_{Lp}|}, \quad \sqrt{1 - s^2} = \frac{v_{Lp}^x}{|\mathbf{v}_{Lp}|} \quad (21)$$

and

$$\chi_L = \frac{|\mathbf{v}_{Lp}|}{v_0}, \quad \chi_{np} = \frac{|\mathbf{v}_{np}|}{v_0} \quad (22)$$

so to rewrite eq. (14) as

$$\begin{aligned} s \chi_L - \chi_{np} + \mathcal{R} \sqrt{1 - s^2} \chi_L^{\beta+1} &= 0 \\ \sqrt{1 - s^2} - \mathcal{R} \chi_L^\beta s &= 0. \end{aligned} \quad (23)$$

Note that $s = \cos(\theta_D)$, where θ_D is the ‘dissipation angle’ introduced by Epstein & Baym (1992), see also Link (2014). Starting from eq. (14) one can show that

$$\begin{aligned} \chi_L &= s \chi_{np} \\ \mathcal{R}^2 \chi_{np}^{2\beta} s^{2\beta+2} + s^2 - 1 &= 0. \end{aligned} \quad (24)$$

Since $0 \leq s \leq 1$, namely $0 \leq \theta_D \leq \pi/2$, we see that the lag between the vortices and the normal component must always be smaller than the lag between the neutron (n) and normal (p) component. It is also interesting to observe that, since $\tilde{\mathcal{R}} = \mathcal{R} \chi_{np}^\beta s^\beta$, the mutual friction coefficient \mathcal{B}_{MF} introduced in eq. (15) reads

$$\mathcal{B}_{MF} = s \sqrt{1 - s^2} = \frac{1}{2} \sin(2\theta_D). \quad (25)$$

Different values of β correspond to different phenomenological models for the dynamics of vortex lines and the evolution of the system will depend on the choice for the index β .

To better discuss this point, let us first remark that it is always possible to choose v_0 such that $\mathcal{R} = 1$, implying $\tilde{\mathcal{R}} \approx 1$ when $|\mathbf{v}_{Lp}| \approx v_0$ (this regime corresponds to the largest possible value for the mutual friction parameter, $\mathcal{B}_{MF} = 1/2$). This value of v_0 defines three velocity ranges $|\mathbf{v}_{Lp}| \ll v_0$, $|\mathbf{v}_{Lp}| \approx v_0$ and $|\mathbf{v}_{Lp}| \gg v_0$, that are related to three mutual friction regimes. This is sketched, for different prescriptions of β , in fig. 1, where we show the dependence of the effective drag parameter $\tilde{\mathcal{R}}$ on $|\mathbf{v}_{Lp}|$, having chosen a fixed value of $\tilde{\mathcal{R}} = 1$ for $|\mathbf{v}_{Lp}| = v_0$.

According to eq. (24), the vortex velocity $|\mathbf{v}_{Lp}|$ decreases as the two components recouple during the spin-up phase of a glitch, simply because the initial lag is decreasing as well.

For $\beta < 0$ and an initial velocity $|\mathbf{v}_{Lp}| > v_0$, the drag increases as the two components recouple and rapidly enters the strong $\tilde{\mathcal{R}} \approx 1$ regime, as we can see for the $\beta = -3/2$ case which is relevant for kelvin mutual friction. If during the recoupling process the lag becomes so small that $|\mathbf{v}_{Lp}| < v_0$, we enter the ‘super-strong’ drag regime, where $\tilde{\mathcal{R}}$ diverges. In this regime the friction coefficient goes to zero as $\mathcal{B}_{MF} \sim \tilde{\mathcal{R}}^{-1}$, so that a negative β could be used to mimic the repinning process, namely a suppression of the mutual friction.

For $\beta > 0$ the opposite is true, and the coupling strength decays (more or less rapidly depending on the actual value of β) as the lag decreases. Such a model, for initial conditions such that $|\mathbf{v}_{Lp}| > v_0$, could be used to describe phenomenologically a situation in which a pinned vortex configuration undergoes unpinning, passes through a phase of strong drag (in which the recoupling of the components is very fast) and possibly a final part in which $|\mathbf{v}_{Lp}| \ll v_0$ and the recoupling proceeds with a much slower timescale.

In fact the power law prescription in eq. (18) can be used to model transitions between different dynamical regimes at different relative vortex velocities. If, for example, one has two microscopic estimates \mathcal{R}_1 and \mathcal{R}_2 for the drag parameter

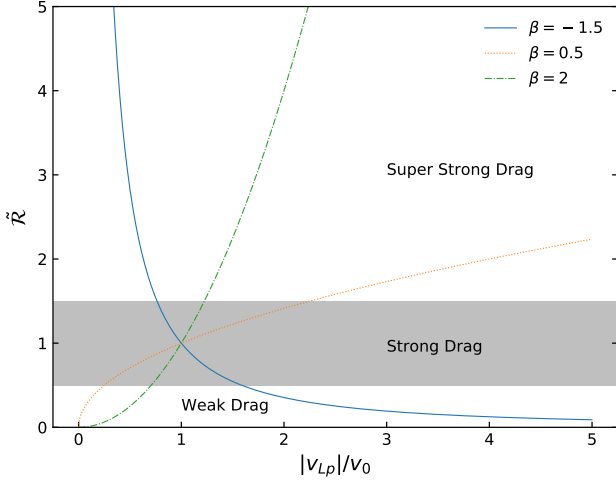


Figure 1. Qualitative plot of the drag parameter $\tilde{\mathcal{R}}$ as a function of $|\mathbf{v}_{Lp}|/v_0$, for different values of β and having chosen a fixed value of $\tilde{\mathcal{R}} = 1$ for $|\mathbf{v}_{Lp}| = v_0$. Three regions are highlighted, the ‘weak drag’ region in which $\mathcal{B}_{MF} \sim \tilde{\mathcal{R}}$, the ‘strong drag’ region in which $\mathcal{B}_{MF} \lesssim 1/2$ and a ‘super strong drag’ one where the mutual friction goes to zero as $\mathcal{B}_{MF} \sim \tilde{\mathcal{R}}^{-1}$. Therefore, a drag force described by a power law with a negative β can be used to model the effect of initially free vortices repinning. For positive values of β the opposite is true, and the coupling becomes weak as $|\mathbf{v}_{Lp}|$ decreases. For the case $\beta = 2$, which describes mutual friction in an isotropic turbulent tangle, the drag is initially strong, but rapidly decreases as the recoupling proceeds.

in two different regimes such that

$$\begin{aligned} \tilde{\mathcal{R}}(\mathbf{v}_{Lp} \approx v_1) &\approx \mathcal{R}_1 = \mathcal{R} \left(\frac{v_1}{v_0} \right)^\beta \\ \tilde{\mathcal{R}}(\mathbf{v}_{Lp} \approx v_2) &\approx \mathcal{R}_2 = \mathcal{R} \left(\frac{v_2}{v_0} \right)^\beta, \end{aligned} \quad (26)$$

we may interpolate between the two values using a power law approximation for the drag with exponent

$$\beta_{12} = \frac{\log(\mathcal{R}_2/\mathcal{R}_1)}{\log(v_2/v_1)}. \quad (27)$$

The final interpolated drag function reads

$$\tilde{\mathcal{R}} = \mathcal{R}_1 \left(\frac{|\mathbf{v}_{Lp}|}{v_1} \right)^{\beta_{12}} = \mathcal{R}_2 \left(\frac{|\mathbf{v}_{Lp}|}{v_2} \right)^{\beta_{12}}. \quad (28)$$

As a result, the choice of a non-linear drag being a simple power law may be used for modelling the transition between different effective drag regimes related to the activation of different dissipation channels, or to model the transition to a strong drag pinned regime.

3.2 Realistic drag in the crust

We now use the methods developed in the previous sections to construct a non-linear model for superfluid drag in the NS crust. Graber et al. (2018) have computed the drag coefficient resulting from Kelvin wave excitations: their estimate of the drag coefficient depends on the typical relative velocity as $\tilde{\mathcal{R}} \propto |\mathbf{v}_{Lp}|^{-3/2}$. On the other hand, Jones (1990a) has shown that Kelvin processes are suppressed below $|\mathbf{v}_{Lp}| \lesssim 500$ cm/s, and that at even lower vortex velocities $|\mathbf{v}_{Lp}| \approx 1$ cm/s the main contribution to the drag comes

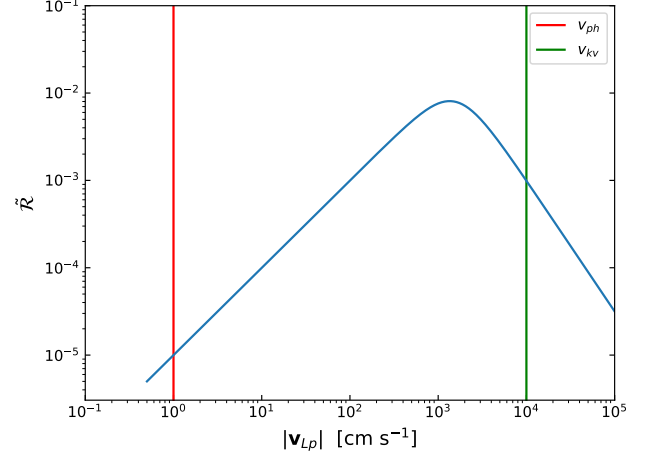


Figure 2. Form of the $\tilde{\mathcal{R}}$ as a function of $|\mathbf{v}_{Lp}|$ where $\mathcal{R}_1 = 10^{-5}$, $\mathcal{R}_2 = 10^{-3}$, $v_1 = 1$ cm/s and $v_2 = 10^4$ cm/s. Since here $\tilde{\mathcal{R}} \ll 1$ we have $\mathcal{B}_{MF} \approx \tilde{\mathcal{R}}$, so that the figure shows with a good accuracy also the behaviour of the mutual friction parameter.

from phonon excitations, leading to a constant coefficient $\mathcal{R} = 10^{-5}$.

Since phonon excitations give rise to a drag coefficient which is lower than the Kelvin one, a realistic model that interpolates between the two behaviours should reduce to

$$\begin{aligned} \tilde{\mathcal{R}} &\approx \mathcal{R}_1 \left(\frac{|\mathbf{v}_{Lp}|}{v_1} \right) & \text{for } v_{Lp} \approx v_1 \ll 500 \text{ cm/s} \\ \tilde{\mathcal{R}} &\approx \mathcal{R}_2 \left(\frac{|\mathbf{v}_{Lp}|}{v_2} \right)^{-3/2} & \text{for } v_{Lp} \approx v_2 \gg 500 \text{ cm/s}, \end{aligned} \quad (29)$$

where v_1 and v_2 are respectively the typical velocities for which the phonon and kelvin excitations are dominant. We choose the simplest linear dependence to get a smooth interpolation between the two channels and the values \mathcal{R}_1 and \mathcal{R}_2 are determined from microphysical calculations of phonon and kelvin drag parameters for $v_{Lp} \approx v_1$ and $v_{Lp} \approx v_2$ respectively.

For our estimate of crustal drag forces we take the constant¹ values $v_1 = 1$ cm/s, with $\mathcal{R}_1 = 10^{-5}$ and $v_2 = 10^4$ cm/s, for which we set $\mathcal{R}_2 = 10^{-3}$. Since there are two power law regimes, we model the transition between them by writing the total drag coefficient as

$$\tilde{\mathcal{R}} = \left(\mathcal{R}_1^{-1} \left(\frac{|\mathbf{v}_{Lp}|}{v_1} \right)^{-1} + \mathcal{R}_2^{-1} \left(\frac{|\mathbf{v}_{Lp}|}{v_2} \right)^{3/2} \right)^{-1}, \quad (30)$$

which is shown as a function of $|\mathbf{v}_{Lp}|$ in fig. 2. Let us stress that the choice of the crossover velocities v_1 and v_2 agrees with microphysical estimates (Jones 1990a; Graber et al.

¹ Clearly, the parameters \mathcal{R}_2 and v_2 vary with density, while here we are not doing so because the glitch model will be rigid (the angular velocity will not depend on the x and z coordinates). Hence, we choose the value of \mathcal{R}_2 and v_2 according to model-A presented in Graber et al. (2018): model-A is the only one for which the estimated value of v_2 lies in the validity regime of kelvonic drag throughout all the crust, namely $v_2 > 10^2$ cm/s⁻¹. According to this model, the value of v_2 varies, while \mathcal{R}_2 is almost constant throughout the whole crust.

2018), but remains, nevertheless, rather uncertain. However, simulations of interactions between vortices and ions in the crust (Wlazlowski et al. 2016) and flux tubes in the core (Drummond & Melatos 2017, 2018) are becoming feasible and more stringent constraints on these parameters may become available in the future.

Introducing dimensionless quantities as in the previous subsection, via eq. (21) and taking

$$\chi_L^{(i)} = \frac{|\mathbf{v}_{Lp}|}{v_i}, \quad \chi_{np}^{(i)} = \frac{|\mathbf{v}_{np}|}{v_i} \quad \text{for } i = 1, 2 \quad (31)$$

where i labels the two crossover velocities, we can write eq. (14) as

$$\begin{aligned} \sqrt{1-s^2} - \left(\mathcal{R}_1^{-1} \chi_L^{(1)-1} + \mathcal{R}_2^{-1} \chi_L^{(2)3/2} \right)^{-1} s &= 0, \\ s \chi_L^{(i)} - \chi_{np}^{(i)} + \left(\mathcal{R}_1^{-1} \chi_L^{(1)-1} + \mathcal{R}_2^{-1} \chi_L^{(2)3/2} \right)^{-1} \sqrt{1-s^2} \chi_L^{(i)} &= 0. \end{aligned} \quad (32)$$

It is then shown that $|v_{Lp}| \leq |v_{np}|$ is still valid, namely $\chi_L^{(i)} = s \chi_{np}^{(i)}$. Hence, it is easy to recast eq. (32) as

$$\left(\frac{1}{\mathcal{R}_1} \left(s \chi_{np}^{(1)} \right)^{-1} + \frac{1}{\mathcal{R}_2} \left(s \chi_{np}^{(1)} \frac{v_1}{v_2} \right)^{3/2} \right)^{-2} s^2 + s^2 - 1 = 0. \quad (33)$$

This equation can now be integrated together with the fluid equations for the system, which we will present in the next section.

4 GLITCH MODEL

Having determined the model for the mutual friction, we investigate its effect on the dynamics of a pulsar glitch. To do this we start from the full equations of motion for the neutron superfluid (n) and normal component (p), which can be written as

$$\begin{aligned} (\partial_t + v_x^j \nabla_j) (v_i^x + \varepsilon_x w_i^{yx}) + \nabla_i (\mu_x + \phi) + \\ + \varepsilon_x w_{yx}^i \nabla_i v_j^x = f_i^x / \rho_x, \end{aligned} \quad (34)$$

where x and y label the chemical component (i.e. $x, y = n, p$), ε_x is the entrainment parameter, μ_x is the chemical potential per unit mass of the substance x , ϕ is the gravitational potential and $w_i^{yx} = v_i^y - v_i^x$ is the relative velocity (see e.g. Prix (2004) and Andersson & Comer (2006)). To build a rigid glitch model we assume axial symmetry (i.e. no dependence on the azimuthal angle φ) and we take the ansatz, with x the cylindrical radius,

$$\mathbf{v}_n = x \Omega_n(t) \hat{e}_\varphi, \quad \mathbf{v}_p = x \Omega_p(t) \hat{e}_\varphi. \quad (35)$$

With this assumption the two fluids equations reduce to

$$\begin{aligned} \partial_t v_i^n + \varepsilon_n \partial_t (v_i^p - v_i^n) + \nabla_i (\mu_n + \phi) &= f_i^n / \rho_n \\ \partial_t v_i^p + \varepsilon_p \partial_t (v_i^n - v_i^p) + \nabla_i (\mu_p + \phi) &= f_i^p / \rho_p. \end{aligned} \quad (36)$$

The ansatz eq. (35) implies that the non-azimuthal components of the two fluid equations in eq. (34) are not dynamical (they represent the hydrostatic equilibrium that sets the structure of the star) and that the continuity equations for the two species are automatically satisfied (Antonelli & Pizzochero 2017).

The force density that enters the two fluid equations is the mutual friction force,

$$f_i^n / \rho_n = F_i^{MF} / \rho_n = -\varepsilon_{ijk} \omega_n^j (v_L^k - v_n^k) \quad (37)$$

Because of the presence of the vorticity ω_n^i in the mutual friction, it is sometimes useful to perform a change of variables and define a new angular velocity given by

$$\Omega_v = (1 - \varepsilon_n) \Omega_n + \varepsilon_n \Omega_p. \quad (38)$$

This quantity is just a variable related to the superfluid momentum that can be used in place of Ω_n and merely represents the total amount of vortices present within the cylindrical radius x via the Feynman-Onsager relation. As a result, the equations of motion in eq. (36) read

$$\begin{aligned} \dot{\Omega}_v &= -2 \Omega_v \frac{v_L^x}{x}, \\ \left(\rho_p - \frac{\varepsilon_n \rho_n}{1 - \varepsilon_n} \right) \dot{\Omega}_p + \frac{\rho_n}{1 - \varepsilon_n} \dot{\Omega}_v &= 0, \end{aligned} \quad (39)$$

where we exploited eq. (8), namely the fact that

$$\boldsymbol{\omega}_n = \frac{1}{m_n} \nabla \times \mathbf{p}_n = 2 \Omega_v \hat{e}_z. \quad (40)$$

These are the equations for a two component rigid glitch model, where the first is a continuity equation for the vortex number (cfr eq. (13) of Antonelli & Pizzochero 2017) while the second is just the angular momentum conservation (i.e. it is equivalent to $\rho_n \dot{\Omega}_n + \rho_p \dot{\Omega}_p = 0$). More precisely, to obtain a well defined averaged rigid model we should average the equations over the whole star, so that the second equation in eq. (39) expresses the conservation of the total angular momentum of the NS,

$$\dot{L}_n + \dot{L}_p = I_n \dot{\Omega}_n + I_p \dot{\Omega}_p = 0. \quad (41)$$

If we now add an external spin down torque α due to electromagnetic emission and use eq. (15), the glitch model equations become

$$\begin{aligned} \dot{\Omega}_v &= -2 \Omega_v \mathcal{B}_{MF} \frac{\Omega_v - \Omega_p}{1 - \varepsilon_n} \\ \dot{\Omega}_p &= -\frac{\alpha}{1 - x_v} - \frac{x_v}{1 - x_v} \dot{\Omega}_v \end{aligned} \quad (42)$$

where we have introduced the fractional moment of inertia $x_x = I_x / I_T$ ($x = p, n$) and $x_v = x_n / (1 - \varepsilon_n)$, while I_T is the total moment of inertia of the star. We also exploited the fact that $\Omega_{vp} = (1 - \varepsilon_n) \Omega_{np}$.

Hence, the form of the equations eq. (42) does not change because of the additional entrainment coupling; moreover, it is possible to include ε_n into the phenomenological parameters. Since our aim is to study the effect of non-linear mutual friction (and as we have shown that the presence of ε_n does not change its form), we will set $\varepsilon_n = 0$ so that eq. (38) reduces to $\Omega_v = \Omega_n$ and $x_v = x_n$.

The p-component here represents the ‘normal’ component, i.e. the proton-electron fluid in the star, the crust, and all components that are coupled to it on a dynamical timescale that is shorter than that of the glitch. In many models it is assumed that, due to electron scattering off magnetised vortex cores (Alpar & Sauls 1988), the superfluid in the core is coupled to the crust fast enough that it can be included in the p component. However, in the outer core the coupling timescale due to mutual friction be comparable to

the rise time (Newton et al. 2015a). This effect has been studied both by integrating the full density dependent equations with also density dependent mutual friction in the core and constant drag in the crust (Haskell et al. 2012; Haskell & Antonopoulou 2014) or by treating the crustal superfluid as an additional component in a three component model with density dependent drag in the crust (Graber et al. 2018). What is observed is that the outer core recouples after the glitch, giving rise to a short term relaxation and possibly an ‘overshoot’, in which the observed frequency rises above the observed long term post-glitch frequency, a behaviour that has indeed been observed in a recent glitch of the Vela pulsar (Ashton et al. 2019; Pizzochero et al. 2019).

In the following we adopt an approximate prescription to model this behaviour by modifying equations eq. (42) to account for a third component - with fractional moment of inertia rx_p - that recouples to the remaining part of the p-component (having fractional moment of inertia $(1-r)x_p$) with a typical timescale τ_{co} . We thus consider the following system of equations

$$\begin{aligned}\dot{\Omega}_n &= -2\mathcal{B}_{MF}\Omega_n(\Omega_n - \Omega_p), \\ x_p(1-r)e^{-t/\tau_{co}}\dot{\Omega}_p + x_n\dot{\Omega}_n &= -\alpha,\end{aligned}\quad (43)$$

which imply that the third component is completely decoupled at $t = 0$: at the beginning of our simulation the effective moment of inertia fraction of the normal component is $x_p(1-r)$, lower than the asymptotic value x_p that is reached at the end of the recoupling. Clearly, the general relation $x_p + x_n = 1$ is still valid.

Following Haskell & Antonopoulou (2014) and Newton et al. (2015b) we will set $r = 0.75$ and choose for τ_{co} the fiducial value of 71 sec so that the latter is compatible with the standard value of the mutual friction coefficient in the core. Later on we will test how a different choice of τ_{co} affects the glitch sizes predicted with this model.

5 NUMERICAL RESULTS: STUDY OF THE GLITCH RISE

To begin our analysis we perform a numerical integration of the two-component model defined by the equations in eq. (42) for the power law ansatz eq. (24). First, we study how the glitch rise time changes with the value of β : the results are shown in fig. 3. Following Seveso et al. (2016), we assume that initially there is a lag between the two fluids of $\Omega_{np} = 10^{-3}$ rad/s, which, for a stellar radius of 10 km, corresponds to a lag of $v_{np} = 10^3$ cm/s in the crust near the equator.

To compare cases corresponding to different values of β , we impose that all models have the same value of $\tilde{\mathcal{R}} = 10^{-3}$ at $t = 0$, so that the initial slope of the rise is equal for each value of β because, initially, the angular momentum is transferred with the same \mathcal{B}_{MF} . We then simulate each model by solving the implicit equation eq. (24) at each integration step so that the evolution of $\tilde{\mathcal{R}}$ and \mathcal{B}_{MF} is peculiar to each model. With the simple power law model we cannot test values of $\beta \leq -1$ (and thus the value $\beta = -3/2$ associated with kelvin waves), because the drag force eq. (19) would diverge when the lag goes to zero, and consequently eq. (24) may not have solutions. This issue is addressed in the more realistic model we will discuss later in this section.

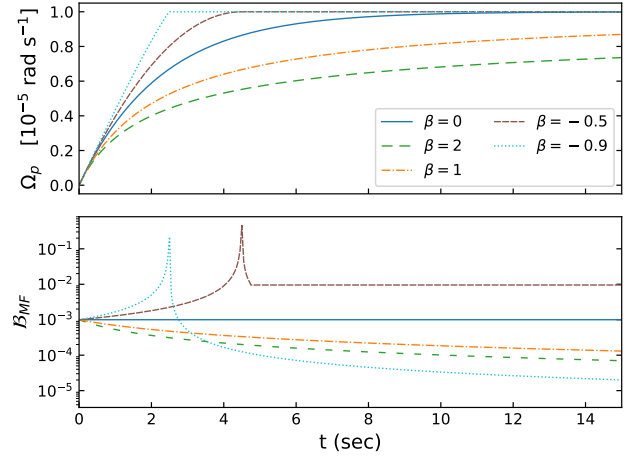


Figure 3. Study of the rise time for a power law drag $\tilde{\mathcal{R}}$ with initial lag $\Omega_{np} = 10^{-3}$ rad/s, $x_p = 0.99$ and torque $\alpha = 10^{-9}$ rad/s².

We observe that for negative values of β the rise is faster than for the usual linear model with $\beta = 0$, which is used here as a reference since it allows to define the exponential timescale for the process. Furthermore, Ω_p grows to the asymptotic value in a finite time because of the rise in the mutual friction coefficient \mathcal{B}_{MF} . Afterwards the value of the \mathcal{B}_{MF} drops sharply (as can be seen in the lower panel of fig. 3) and the frequency evolution essentially stops. On the contrary, for positive values of β the rise is much gentler because the angular momentum transfer rate decreases with the lag; we also observe that, for values of β high enough, this may result in smaller glitches when the time taken for the rise becomes longer than the spin down typical timescale. This effect can be seen in fig. 4 for the $\beta = 2$ case, where the integration is performed long enough that the spin-down torque effects become apparent.

The behaviour for negative values of β , for which we observe a very rapid rise, is consistent with observations of recent glitches in the Crab pulsar, and also with a recent large glitch in the Vela pulsar, for which an upper limit on the rise time of 12 s was set at the 90% confidence level, with the data favouring, in general, very short rise times (Ashton et al. 2019). It is therefore clear that to obtain quantitative constraints on interior NS physics it is not sufficient to calculate drag coefficients for a fixed $|\mathbf{v}_{Lp}|$ and then treat them as constants to obtain an exponential rise, as the behaviour inferred from timing observations is qualitatively different.

We now turn our attention to the more microphysical prescription for the drag given in eq. (30) and plotted in fig. 2, which allows for both kelvin and phonon contributions in the NS crust.

From our previous analysis of the power law case, we expect to have different behaviours for the glitch rise if the initial lag is larger or smaller than the value for which the maximum of \mathcal{B}_{MF} occurs, i.e. if the drag is in the negative β regime for high values of $|\mathbf{v}_{Lp}|$, or in the positive β regime for low values of $|\mathbf{v}_{Lp}|$.

To investigate this we integrate the two-component model for different initial conditions, for initial values of $v_{np} = R\Omega_{np}$ both before and after the peak of \mathcal{B}_{MF} . Ex-

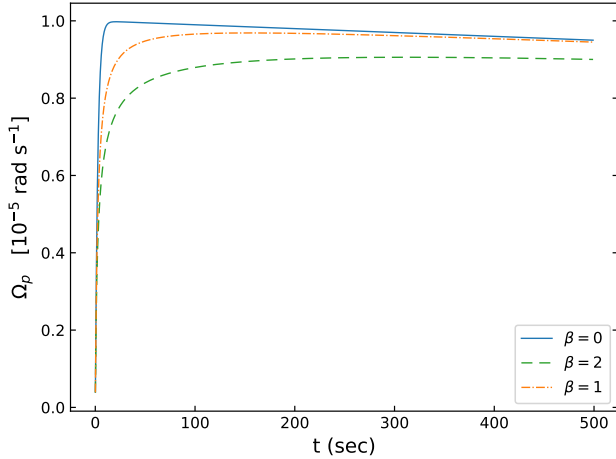


Figure 4. Long time evolution for positive β , in which we verify that the value of the glitch amplitude after the first minutes is not necessarily the same for all cases. The initial lag used is $\Omega_{np} = 10^{-3}$ rad/s, $I_p/I_T = 0.99$ and torque $\alpha = 10^{-9}$ rad/s².

amples of the results are shown in figs. 5 to 7. In the case with a large lag at $t = 0$ that falls in the $\beta < 0$ part of the drag, we can observe a change in the convexity of the rise in correspondence of the activation of the phonon dissipation channel, see fig. 5. In these cases the initial rise is very rapid, and likely to decouple part of the core, causing an ‘overshoot’ and rapid post-glitch recoupling, as expected in some glitch models (see e.g. Haskell et al. 2012; Antonelli & Pizzochero 2017; Graber et al. 2018; Pizzochero et al. 2019). For small values of the initial lag, on the other hand, only values of $\beta > 0$ are sampled, and the mutual friction strength drops off as the glitch proceeds. Like in the previous simpler case, this behaviour can possibly lead to smaller amplitude glitches, as the coupling timescale becomes long enough to be comparable to the spin-down timescale and the rise is effectively halted.

6 NUMERICAL RESULTS: GLITCH SIZE DISTRIBUTIONS

In the previous section we mostly focused on the effects of the microscopic drag in eq. (30) on the glitch rise, namely on the first few seconds after the glitch is started. The same friction model can also be used to study the long time frequency evolution of the star after a glitch, and also glitch sizes. The frequency evolution is ultimately determined once the initial lag, and consequently the initial coupling timescale between the two components, is chosen. This quantity is not constrained, and may vary from glitch to glitch even in the same star. Therefore, we now study the glitch size distributions that we get out of the model for an initial lag in the interval $[10 : 10^5]$ cm/s, see fig. 8.

First, we observe that for large initial lags the drag is mainly due to Kelvin excitations and increases as the system recouples, leading to a very rapid rise. This in turn may decouple part of the core and lead to a larger initial jump in frequency. To investigate this effect we consider the approximate 3-component model in section 3.2, in which the core

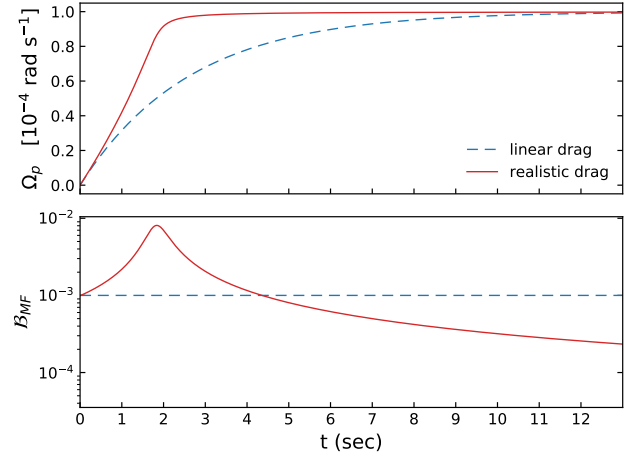


Figure 5. Glitch rise (red, solid) for the microscopic drag prescription in eq. (30) compared to the exponential rise given by linear mutual friction (blue, dashed) for $x_p = 0.99$. The initial lag is $\Delta\Omega_{np} = 10^{-2}$ rad/s, larger than the value for which the maximum of \mathcal{B}_{MF} occurs.

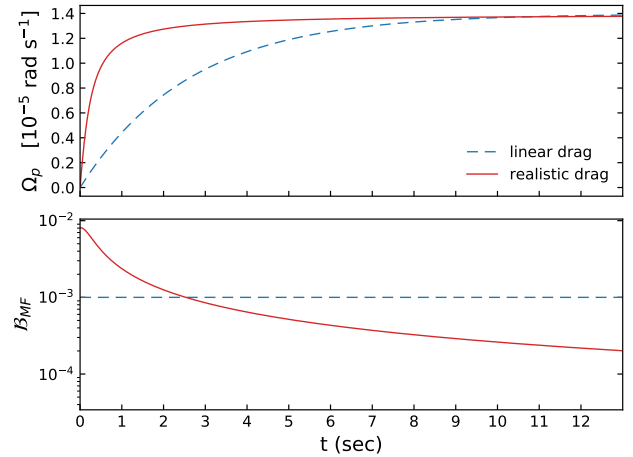


Figure 6. Glitch rise (red, solid) for the microscopic drag prescription in eq. (30) compared to the exponential rise given by linear mutual friction (blue, dashed) for $x_p = 0.99$. The initial lag is $\Omega_{np} = 1.4 \times 10^{-3}$ rad/s that corresponds to the value for which the maximum of \mathcal{B}_{MF} occurs.

recouples with a timescale τ_{co} . This means that the angular momentum is transferred to an observable p-component with smaller inertia and results in larger glitches (although note that it will not reproduce an overshoot as a full 3-component model such as that of Graber et al. (2018) or Pizzochero et al. (2019)). The effect is more evident for large initial lags for which angular momentum is transferred more rapidly (\mathcal{B}_{MF} higher) and the fraction of core that has already recoupled is smaller.

The initial condition have been chosen to be consistent with parameters of the Vela pulsar, so that $\Omega_p(0) \approx \Omega_n(0) = 70.34$ rad/s and $\alpha = 9.8 \cdot 10^{-11}$ rad/s². Also, in order to test the effects of the of τ_{co} we consider the fiducial value for Vela (see Haskell & Antonopoulou 2014; Newton et al. 2015b),

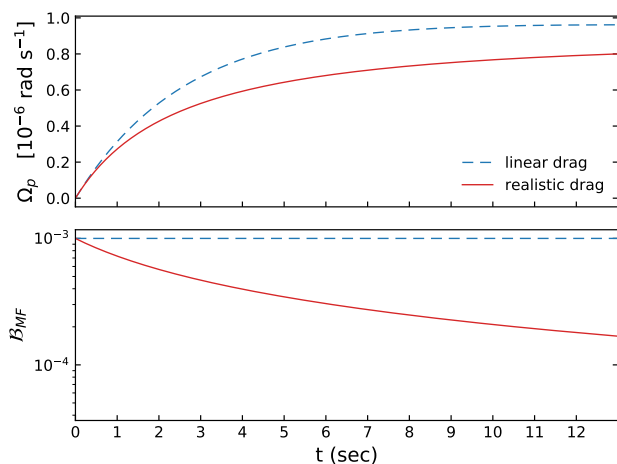


Figure 7. Glitch rise (red, solid) for the microscopic drag prescription in eq. (30) compared to the exponential rise given by linear mutual friction (blue, dashed) for $x_p = 0.99$. The initial lag is $\Omega_{np} = 10^{-4} \text{ rad/s}$ and thus smaller than the value for which the maximum of \mathcal{B}_{MF} occurs.

namely $\tau_{co} = 71 \text{ s}$, but also $\tau_{co} = 7.1 \text{ s}$ which is compatible with the linear model timescale and $\tau_{co} = 710 \text{ s}$. Throughout this entire section the glitch is computed from the residuals, namely as $\Omega_p(t) - \Omega_p(0) + \alpha t$, where α is the absolute value of the spin down rate, because this is compatible with the observational procedure.

As a first step we consider initially a log-uniform distribution of the initial lags v_{np} in the range $[10; 10^5] \text{ cm/s}$, see fig. 8. The output glitch distribution in the linear case is presented in fig. 9: as expected the output distributions are flat as well and roughly scaled by a factor $x_n = 0.01$, while the only effect of the approximate three component model is to slightly shift the glitch sizes to bigger values. Furthermore, since in the linear model the angular momentum is transferred at a constant rate, the effects of the approximate 3-component model are the same for each initial lag, namely the output glitch-size distribution is “rigidly” shifted to the right by a greater amount for larger values of τ_{co} .

In fig. 10 we compare the output glitch distribution for the standard linear drag 2-component model with the ones obtained using the realistic non-linear drag from section 3.2 and assuming to “measure” the glitch after 200 s. We see that now in all cases with non zero τ_{co} the output distributions present a peak for high glitches, and while there is a quantitative difference between the different cases, the qualitative feature is present in all the three models. To point out that this effect is due to the modified mutual friction - and not to the effect of the third component, so that it must be visible even in the $\tau_{co} = 0$ case - in fig. 11 we plot the output distribution that we get if we “measure” the glitch after 50 sec. Note that the latter is compatible with the current observational limits on the full glitch rise time (Dodson et al. 2002), although the initial rise may be of the order of 12 s (Ashton et al. 2019). In fig. 11 the peak is in fact present also for the non-linear $\tau_{co} = 0 \text{ sec}$ model. This feature is interpreted as follows: for very high initial lags, namely $v_{np} \approx 10^5 \text{ cm/s}$, the system is sampling the area well right to the peak of the \mathcal{B}_{MF} plot (see fig. 2), so that we have a considerably low

value for the initial angular momentum transfer rate. This implies that the angular momentum reservoir is not completely emptied out within 50 s and we measure a smaller glitch size. The system is sampling the kelvonic branch, so that the rate increases as the system recouples and the residual is transferred within the next 150 s in the $\tau_{co} = 0$ case - and can possibly be considered as a delayed rise². If we consider the approximate 3-component model, the dynamics depends on the interplay between two “timescales”, the angular momentum transfer rate (which changes during the evolution) and τ_{co} . As a result, we still observe the peak after 200 s. As expected, the microscopic drag of eq. (30) gives also smaller glitches (with respect to the linear case) when the system samples the phonon-branch only, namely for low initial lags³. This effect is counteracted in the approximate three component model and in the fiducial model (the one with $\tau_{co} = 71 \text{ s}$) we observe a reduction in the number of small glitches, see fig. 10.

In fig. 12 we test a somewhat more realistic scenario in which the initial lag distribution is not log-uniform but follows a power law with exponent -1.2 as suggested by both simulations of vortex avalanches (Warszawski & Melatos 2012) and observations of pulsar glitch size distributions (Howitt et al. 2018; Melatos et al. 2008), see fig. 8. The features discussed in the previous log-uniform case are still present, but now we are sampling smaller values for the initial lags with higher probability. In this case the distribution turns out to be bimodal, with a narrower larger size component above approximately $10^2 \mu\text{Hz}$ and a wider second component extending to lower sizes. This distribution is in qualitative agreement with the observed distribution presented by Fuentes et al. (2017) and Ashton et al. (2017), which suggests that the same mechanism (the recoupling of a pinned superfluid) can explain both populations if a non-linear drag model is used.

It is thus possible that in NSs with predominantly large glitches (like the Vela pulsar) the events are triggered in stronger pinning regions, while in stars with a majority of smaller glitches, these are likely to be triggered in weaker pinning regions. This is in agreement with the analysis of Haskell et al. (2018b), according to which larger glitches are likely to be triggered in the outer core of the star.

However, to obtain more stringent constraints future work should include corrections due to general relativity (see e.g. Sourie et al. 2017; Antonelli et al. 2018; Gavassino et al. 2020) and the full density dependence of the drag in the core (Alpar et al. 1984; Andersson & Comer 2006) and crust of the star Graber et al. (2018).

7 CONCLUSIONS

We studied the effect of a non-linear form of the mutual friction on pulsar glitch sizes and rise times: we considered both a simple power law dependence of the drag force on

² The delayed rise in the largest glitch observed in Crab pulsar (see Shaw et al. 2018) could be the effect of a non-linear mutual friction (but with model parameters different from those considered in the present work).

³ Recall that $v_{Lp} \leq v_{np}$, so that for small initial lag the system is sampling the region left to the \mathcal{B}_{MF} peak, see fig. 2.

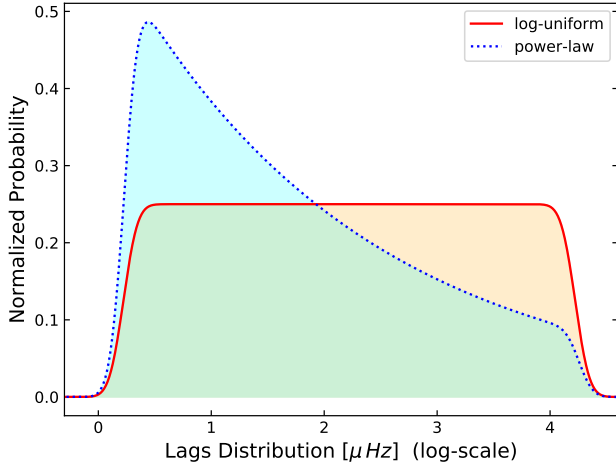


Figure 8. Input distributions of the initial lags for the two cases of interest: log-uniform (red, solid) in the interval $[10 : 10^5]$ cm/s and power law (blue, dashed) in the same interval with exponent -1.2 .

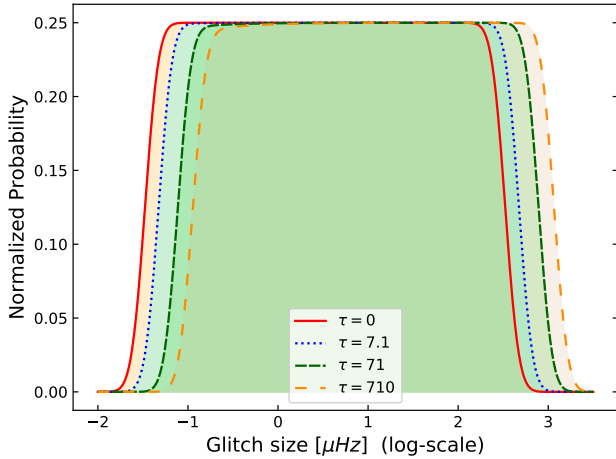


Figure 9. Output glitch size distribution in the linear case for an initial (log-scale) uniform lags distribution. The linear $\tau = 0$ case (red, solid) is given for comparison with the approximate 3-component ones: $\tau = 7.1$ (blue, dotted), $\tau = 71$ (green, dashed) and $\tau = 710$ (yellow, dashed).

the relative velocity between superfluid vortices and the normal component, and a physically motivated model for the crust of a NS, in which for low vortex velocities the drag is mainly due to phonon excitations while for high velocities to kelvin excitations (Jones 1990a, 1992; Epstein & Baym 1992; Graber et al. 2018).

For the simple power law case we find that for positive values of the index β the rise is slower than in the standard linear case, for which the rise is exponential. This case is relevant for both classical turbulence, for which one expects a power law index $\beta = 1$ and isotropic quantum turbulence for which $\beta = 2$ and confirms the previous results of Peralta et al. (2006) for the rise time. Additionally we find that for $\beta > 0$ the size of the glitch can also be affected, as

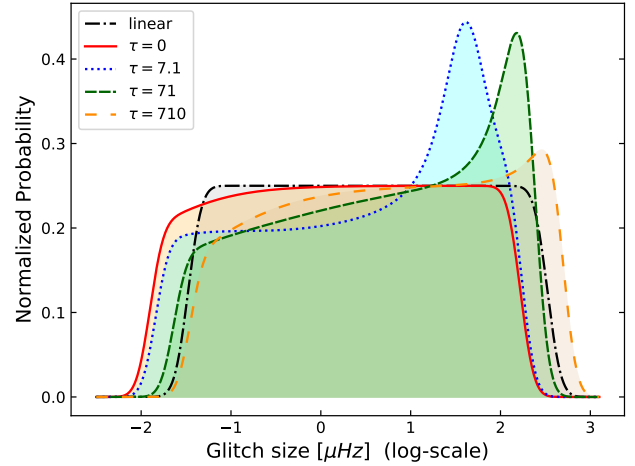


Figure 10. Comparison of glitch size distributions in the linear and realistic non-linear case for an initial log-uniform lags distribution. The linear case (black, dash-dotted) is given for comparison with the non-linear 2-component model (red, solid) and approximate 3-component ones: $\tau = 7.1$ s (blue, dotted), $\tau = 71$ s (green, dashed) and $\tau_{co} = 710$ s (yellow, dashed). The glitch is measured at 200 sec.

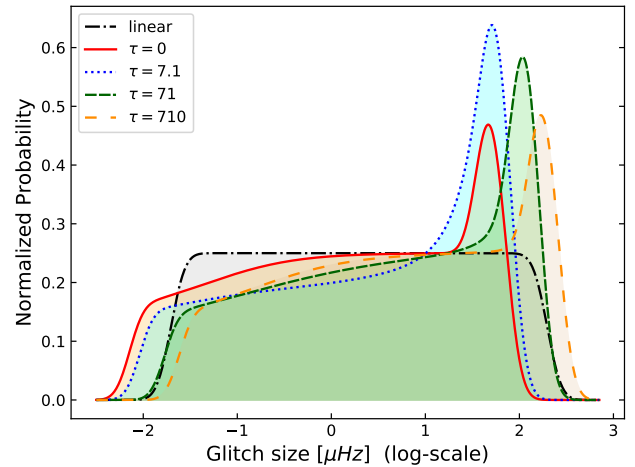


Figure 11. Comparison of glitch size distributions in the linear and realistic non-linear case for an initial log-uniform lags distribution. The linear case (black, dash-dotted) is given for comparison with the non-linear 2-component model (red, solid) and approximate 3-component ones: $\tau = 7.1$ s (blue, dotted), $\tau = 71$ s (green, dashed) and $\tau_{co} = 710$ s (yellow, dashed). The glitch is measured at 50 sec.

the coupling timescale rapidly grows to the point where it is comparable to the spindown timescale, thus effectively halting the rise and leading to smaller glitches.

For negative values of the power law index β the situation is reversed, and the drag parameter \tilde{R} grows as the vortices slowdown. This is particularly relevant for glitches, as the rapid rise is thought to be due to mutual friction coupling given by the excitation of Kelvin waves either in the crust, as vortices move past the ions in the lattice, or core, as they cut through superconducting fluxtubes (Ruderman

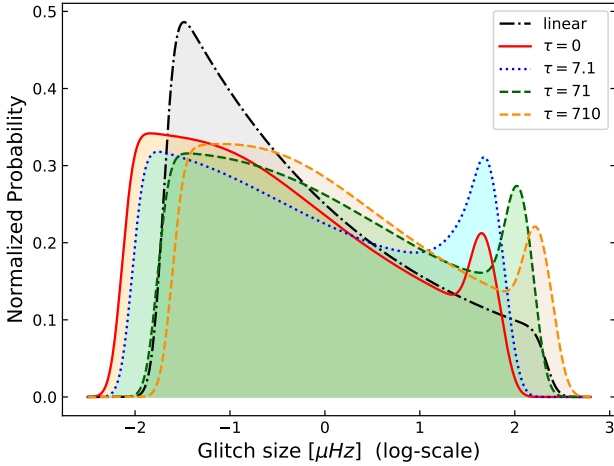


Figure 12. Comparison of glitch size distributions in the linear and realistic non-linear case for an initial power law lags distribution. The linear case (black, dash-dotted) is given for comparison with the non-linear 2-component mode (red, solid) and two approximate 3-component ones: $\tau = 7.1$ s (blue, dotted), $\tau = 71$ s (green, dashed) and $\tau_{co} = 710$ s (yellow, dashed). The power law exponent is -1.2 and the glitch is measured at 50 sec.

et al. 1998; Link 2003). In both the cases where the dissipation is due to excitation of Kelvin waves the expected index is expected to be $\beta = -3/2$.

In the more realistic model defined in eq. (30) we have that at high velocities (above $v_0 \approx 10^3$ cm/s) vortices experience a kelvonic drag that scales as $v_{LP}^{-3/2}$, while at lower velocities the kelvonic contributions are suppressed and phonons dominate the drag, scaling as v_{LP} (Jones 1990a). This means that for high initial lags (corresponding to strong pinning regions) vortices experience an initially increasing drag after the depinning, as in the $\beta < 0$ power law case. On the contrary, for low initial lags only $\beta > 0$ regions are sampled, see fig. 2. We explore the effect of this drag model on the observed glitch size distribution with both our standard 2-component model, and also with an approximate 3-component model. In both cases the observed glitch distribution presents an excess of large glitches. This automatically implies that, given an input distribution that favors small initial lags (Howitt et al. 2018), the observed glitch distribution is bimodal, with a narrower peak above $\Delta\nu_{glitch} \approx 10^2 \mu\text{Hz}$ and a wider component for lower sizes. This is qualitatively consistent with what is observed in the pulsar population (Fuentes et al. 2017). It is thus possible that both populations of glitches (i.e. the ‘large’ and ‘small’ glitches) originate from the same mechanism, namely the re-coupling of a pinned superfluid component, once the realistic kelvin-phonon mutual friction is considered.

Furthermore, we speculate that the different size distributions observed in individual pulsars may be due to the glitch originating in different regions of pinned vorticity. For pulsars where power law distributions are observed, it is likely that the glitch originates in regions where the pinning is not strong enough to allow for large initial lags (i.e. regions in which the typical lags before unpinning are not large enough to allow the vortex to experience the kelvonic,

$\beta = -3/2$, branch of the mutual friction). On the other hand, in pulsars that glitch quasi-periodically with a preferred size, such as the Vela or J0537-6910, it is likely that glitches occur in strong pinning regions where only kelvonic mutual friction is present. This would be the case in the outer core, where vortex-flux tube interactions allow for strong pinning (Sourie & Chamel 2020), but will also excite Kelvin waves on the vortices once they are free to cut through the flux tubes (Ruderman et al. 1998; Link 2003).

In conclusion we have shown that non-linear mutual friction in NS interiors leads to appreciable differences in pulsar glitch rises compared to the standard linear model. In particular, a non-linear drag that interpolates between the phononic and kelvonic regimes allows to explain the differences observed in the size distributions in terms of a single process and is also consistent with recently observed glitches in the Crab and Vela pulsar (Haskell et al. 2018b). To obtain constraints on the EOS, on transport parameters in the NS interior and on the glitch trigger region, however, future work should aim to include the effect of general relativity (Sourie et al. 2017; Antonelli et al. 2018; Gavassino et al. 2020), and to make contact with microphysical calculations of interactions between vortices and ions in the NS crust (Seveso et al. 2016; Wlazlowski et al. 2016). This will allow to study how structural differences between glitching pulsars affect their glitch size distribution, and to constrain microphysical parameters in the high density interior of the star (Ho et al. 2015; Pizzochero et al. 2017; Montoli et al. 2020).

ACKNOWLEDGEMENTS

T.C. acknowledges support from PHAROS COST Action (CA16214). V.K., M.A. and B.H. acknowledge support from the Polish National Science Centre grant SONATA BIS 2015/18/E/ST9/00577, P.I.: B. Haskell. This research was supported in part by the INT’s U.S. Department of Energy grant No. DE-FG02-00ER41132. The authors thank N. Andersson for reading the manuscript and useful critical comments.

REFERENCES

- Abbott B. P., Abbott R., Abbott T. D., Acernese F., 2018, *Phys. Rev. Lett.*, 121, 161101
- Alpar M. A., 2017, *Journal of Astrophysics and Astronomy*, 38, 44
- Alpar M. A., Sauls J. A., 1988, *ApJ*, 327, 723
- Alpar M. A., Langer S. A., Sauls J. A., 1984, *ApJ*, 282, 533
- Anderson P. W., Itoh N., 1975, *Nature*, 256, 25
- Andersson N., Comer G. L., 2006, *Class. Quantum Gravity*, 23, 5505
- Andersson N., Sidery T., Comer G. L., 2006, *Monthly Notices of the Royal Astronomical Society*, 368, 162
- Andersson N., Sidery T., Comer G. L., 2007, *Monthly Notices of the Royal Astronomical Society*, 381, 747
- Andersson N., Glampedakis K., Ho W. C. G., Espinoza C. M., 2012, *Physical Review Letters*, 109, 241103
- Antonelli M., Pizzochero P. M., 2017, *Mon. Not. R. Astron. Soc.*, 464, 721
- Antonelli M., Montoli A., Pizzochero P. M., 2018, *MNRAS*, 475, 5403

- Antonopoulou D., Espinoza C. M., Kuiper L., Andersson N., 2018, *MNRAS*, **473**, 1644
- Ashton G., Prix R., Jones D. I., 2017, *Physical Review D*, **96**, 063004
- Ashton G., Lasky P. D., Graber V., Palfreyman J., 2019, *Nature Astronomy*, p. 417
- Baym G., Chandler E., 1983, *Journal of Low Temperature Physics*, **50**, 57
- Bekarevich I. L., Khalatnikov I. M., 1961, *Sov.Phys. JETP*, **13**, 643
- Bogdanov S., et al., 2019, *BAAS*, **51**, 506
- Carter B., Chamel N., 2005, *International Journal of Modern Physics D*, **14**, 749
- Carter B., Chamel N., Haensel P., 2006, *Int. J. Mod. Phys. D*, **15**, 777
- Chamel N., 2012, *Phys. Rev. C*, **85**, 035801
- Chamel N., 2013, *Phys. Rev. Lett.*, **110**, 011101
- Chamel N., 2017, *Journal of Astrophysics and Astronomy*, **38**, 43
- Delsate T., Chamel N., G rlebeck N., Fantina A. F., Pearson J. M., Ducoin C., 2016, *Physical Review D*, **94**, 023008
- Dodson R. G., McCulloch P. M., Lewis D. R., 2002, *ApJ, Letters*, **564**, L85
- Donnelly R. J., 1991, *Quantized Vortices in Helium II*. Cambridge University Press, 1991
- Drummond L. V., Melatos A., 2017, *MNRAS*, **472**, 4851
- Drummond L. V., Melatos A., 2018, *MNRAS*, **475**, 910
- Epstein R. I., Baym G., 1992, *Astrophys. J.*, **387**, 276
- Fuentes J. R., Espinoza C. M., Reisenegger A., Stappers B. W., Shaw B., Lyne A. G., 2017, preprint, ([arXiv:1710.00952](https://arxiv.org/abs/1710.00952))
- Fulgenzi W., Melatos A., Hughes B. D., 2017, *MNRAS*, **470**, 4307
- Gavassino L., Antonelli M., Pizzochero P., Haskell B., 2020, eprint, [arXiv:2001.08951](https://arxiv.org/abs/2001.08951)
- Glampedakis K., Andersson N., Samuelsson L., 2011, *MNRAS*, **410**, 805
- Graber V., Cumming A., Andersson N., 2018, *ApJ*, **865**, 23
- Haensel P., Potekhin A. Y., Yakovlev D. G., 2007, *Neutron stars 1: Equation of state and structure*. Vol. 326, Springer, New York, USA, doi:10.1007/978-0-387-47301-7
- Hall H. E., Vinen W. F., 1956, *Proceedings of the Royal Society of London Series A*, **238**, 215
- Haskell B., Antonopoulou D., 2014, *MNRAS*, **438**, L16
- Haskell B., Melatos A., 2015, *International Journal of Modern Physics D*, **24**, 1530008
- Haskell B., Sedrakian A., 2017, preprint, ([arXiv:1709.10340](https://arxiv.org/abs/1709.10340))
- Haskell B., Pizzochero P. M., Sidery T., 2012, *Monthly Notices of the Royal Astronomical Society*, **420**, 658
- Haskell B., Glampedakis K., Andersson N., 2014, *MNRAS*, **441**, 1662
- Haskell B., Khomenko V., Antonelli M., Antonopoulou D., 2018a, *MNRAS*, **481**, L146
- Haskell B., Khomenko V., Antonelli M., Antonopoulou D., 2018b, *Mon. Not. Roy. Astron. Soc.*, **481**, L146
- Ho W. C. G., Espinoza C. M., Antonopoulou D., Andersson N., 2015, *Science advances*, **1**, e1500578
- Howitt G., Melatos A., Delaigle A., 2018, *ApJ*, **867**, 60
- Jones P. B., 1990a, *Mon. Not. R. Astron. Soc.*, **243**, 257
- Jones P. B., 1990b, *MNRAS*, **244**, 675
- Jones P. B., 1992, *Mon. Not. R. Astron. Soc.*, **257**, 501
- Khomenko V., Haskell B., 2018, *Publ. Astron. Soc. Australia*, **35**, e020
- Khomenko V., Antonelli M., Haskell B., 2019, *Phys. Rev. D*, **100**, 123002
- Langlois D., Sedrakian D. M., Carter B., 1998, *Mon. Not. R. Astron. Soc.*, **297**, 1189
- Link B., 2003, *Phys. Rev. Lett.*, **91**, 101101
- Link B., 2014, *The Astrophysical Journal*, **789**, 141
- Lyne A. G., Jordan C. A., Graham-Smith F., Espinoza C. M., Stappers B. W., Weltevred P., 2015, *MNRAS*, **446**, 857
- Melatos A., Peralta C., 2007, *Astrophysical Journal, Letters*, **662**, L99
- Melatos A., Peralta C., Wyithe J. S. B., 2008, *ApJ*, **672**, 1103
- Mendell G., 1991, *ApJ*, **380**, 530
- Mongiovi M. S., Jou D., 2007, *Phys. Rev. B*, **75**, 024507
- Montoli A., Antonelli M., Pizzochero P. M., 2020, *Monthly Notices of the Royal Astronomical Society*, **492**, 4837
- Muslimov A. G., Tsygan A. I., 1985, *Ap&SS*, **115**, 43
- Newton W. G., Berger S., Haskell B., 2015a, *Mon. Not. R. Astron. Soc.*, **454**, 4400
- Newton W. G., Berger S., Haskell B., 2015b, *MNRAS*, **454**, 4400
- Palfreyman J., Dickey J. M., Hotan A., Ellingsen S., van Straten W., 2018, *Nature*, **556**, 219
- Peralta C., Melatos A., Giacobello M., Ooi A., 2006, *ApJ*, **651**, 1079
- Pizzochero P. M., Antonelli M., Haskell B., Seveso S., 2017, *Nature Astronomy*, **1**, 0134
- Pizzochero P., Montoli A., Antonelli M., 2019, arXiv e-prints, p. [arXiv:1910.00066](https://arxiv.org/abs/1910.00066)
- Prix R., 2004, *Phys. Rev. D*, **69**, 043001
- Prix R., Comer G. L., Andersson N., 2002, *Astronomy and Astrophysics*, **381**, 178
- Ruderman M., Zhu T., Chen K., 1998, *Astrophys. J.*, **492**, 267
- Schwarz K. W., 1988, *Phys. Rev. B*, **38**, 2398
- Seveso S., Pizzochero P. M., Grill F., Haskell B., 2016, *Mon. Not. R. Astron. Soc.*, **455**, 3952
- Shaw B., et al., 2018, *MNRAS*, **478**, 3832
- Simula T., 2018, *Phys. Rev. A*, **97**, 023609
- Sonin E. B., 1987, *Rev. Mod. Phys.*, **59**, 87
- Sourie A., Chamel N., 2020, *Monthly Notices of the Royal Astronomical Society*
- Sourie A., Chamel N., Novak J., Oertel M., 2017, *MNRAS*, **464**, 4641
- Srinivasan G., Bhattacharya D., Muslimov A. G., Tsygan A. J., 1990, *Current Science*, **59**, 31
- Vinen W. F., 1957, *Proceedings of the Royal Society of London Series A*, **242**, 493
- Warszawski L., Melatos A., 2012, *Mon. Not. R. Astron. Soc.*, **428**, 1911
- Wlazlowski G., Sekizawa K., Magierski P., Bulgac A., Forbes M. M. N., 2016, *Physical Review Letters*, **117**

This paper has been typeset from a \LaTeX file prepared by the author.